Genesis of "Solitary Cations" Induced by Atomic Hydrogen

Giorgio Pettinari, Francesco Filippone,* Antonio Polimeni, Giuseppe Mattioli, Amalia Patanè, Vladim Lebedev, Mario Capizzi, and Aldo Amore Bonapasta*

Substitution of constituent atoms and/or changes of crystal structure are routinely used to tailor the fundamental properties of a semiconductor. Here, it is shown that such a tailoring can also be realized thanks to a novel hydrogen effect. Four hydrogen atoms can screen the effect the crystal potential has on a constituent cation, thus generating a *solitary cation*: an effectively isolated impurity, so chemically different from the unscreened constituent cations that it strongly perturbs the electronic properties of the material by increasing its *fundamental* band-gap energy. Such a hydrogen-induced screening effect is removed by thermal treatments, thus permitting reversible modifications of both the "crystal chemistry" and material's properties. This phenomenon, observed in InN and other topical nitrides, should permit the development of a new class of materials as well as the fabrication of photonic devices and optical integrated circuits with distinct, tailor-made regions emitting or absorbing light, all integrated onto a monolithic semiconductor structure.

1. Introduction

Research in semiconductors has often aimed at controlling the electronic and/or optical properties of a material by suitable changes in its chemical composition or crystal structure. This goal has been commonly pursued through the introduction of foreign atoms (namely by doping or alloying) or defect structures (e.g., crystal vacancies) into the host lattice. In the tuning of semiconductor's properties an important role has also been and it is still played by atomic hydrogen. The small size of hydrogen, which is a ubiquitous element in many semiconductor growth techniques and device processing steps, promotes its diffusion into the host lattice, where it can interact with impurities and defects by forming complexes involving constituent and/or foreign atoms and sizably modify or even neutralize their effects on the host material.[1–4] While these properties of hydrogen are well known and have been widely investigated in the literature, it has never been reported that hydrogen incorporation in a semiconductor crystal *modifies the chemistry of its constituent atoms*. Here, we describe this unique phenomenon—to which we refer to as *"genesis of solitary cations"*—and demonstrate that it can induce remarkable changes in the fundamental electronic properties of several nitride semiconductors. For instance, in the case of InN, a constituent In cation can be isolated from its crystalline environment through the formation of strong N—H bonds between its four N-neighbors and four hydrogen atoms. Such an In solitary cation—an isolated "impurity" generated by an effective screening of the crystal environment—induces a band anticrossing effect, thus significantly contributing to an increase in the material's band-gap energy by as much as 0.4 eV. This is a *genuine* band-gap opening, thoroughly different from the Moss–Burstein shift induced by a formation of H-related donors.[5,6] Generally, a distinctive feature of the formation of H-complexes in a semiconductor lattice is their controllable dissociation under suitable thermal procedures.[1,2] This holds also for the multihydrogen complex responsible for the genesis of the solitary cations. The effects of atomic hydrogen on the fundamental properties of InN—also observed in In-rich (InGa)N alloys and predicted in GaN—represent a singular and unexpected physical phenomenon. Moreover, the genesis and vanishing of solitary cations offer opportunities for innovative technologies in semiconductors. They indicate a way of tuning the optical properties of nitrides via a spatially controlled incorporation or removal of H-atoms,[7,8] that can lead to photonic devices and optical integrated circuits with distinct, tailor-made regions emitting or absorbing light all integrated onto a monolithic semiconductor structure.

Dr. G. Pettinari
National Research Council
Institute for Photonics and Nanotechnologies (IFN-CNR)
Via Cineto Romano 42, 00156 Roma, Italy
E-mail: giorgio.pettinari@cnr.it
Dr. F. Filippone, Dr. G. Mattioli, Dr. A. Amore Bonapasta
National Research Council
Istituto di Struttura della Materia (ISM-CNR)
Via Salaria Km 29.5, 00016 Monterotondo Stazione, Italy
E-mail: francesco.filippone@ism.cnr.it
Dr. G. Pettinari, Prof. A. Polimeni, Prof. M. Capizzi
Physics Department
Sapienza University of Rome
P.le A. Moro 2, 00185 Roma, Italy
Dr. G. Pettinari, Prof. A. Patanè
School of Physics and Astronomy
The University of Nottingham
Nottingham NG7 2RD, UK
Dr. V. Lebedev
Fraunhofer Institute for Applied Solid State Physics
Tullastraße 72, 79108 Freiburg, Germany

The copyright line of this paper was amended 30 November 2015.

DOI: 10.1002/adfm.201501858

2. Results and Discussion

2.1. Experimental Observations

The effects of solitary cations in InN are revealed by changes in the photoluminescence (PL) spectra upon incorporation of

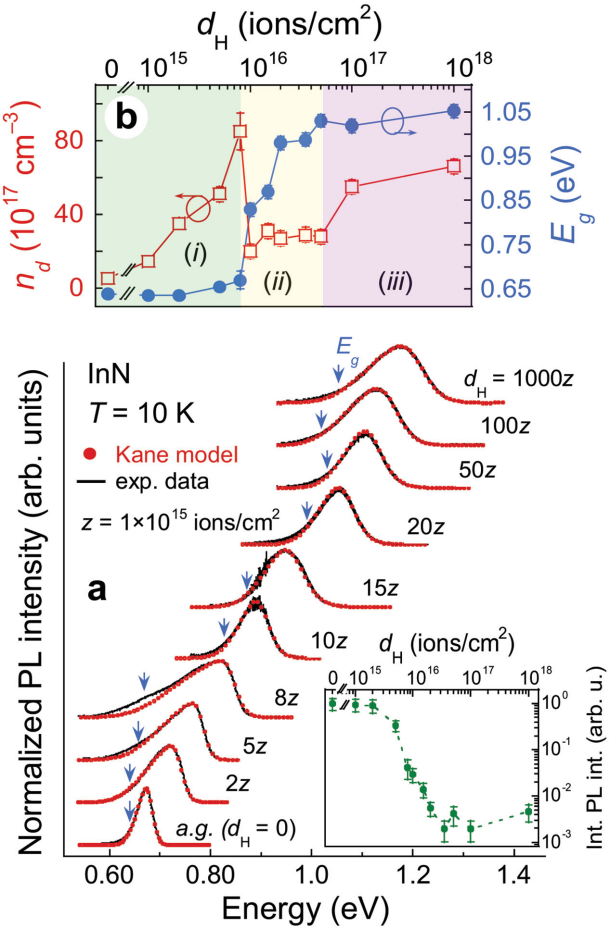

Figure 1. Band-gap opening in hydrogenated InN. a) Low-temperature (T = 10 K) normalized PL spectra (solid lines) of an InN epilayer post-growth treated with increasing H-doses (d_H). Features at ≈0.9 eV are due to atmospheric absorption. The integrated PL intensity is shown in the inset. Simulations of PL spectra in terms of a Kane semiclassical model (see text and ref.[9] are given by full dots. b) Estimated values of the renormalized band-gap energy (E_g) and donor-induced carrier density (n_d) as a function of d_H. Shaded colored areas identify the three d_H regions described in the text.

increasing H-doses (d_H), as shown in **Figure 1**. Spectra simulations, as performed within the Kane semiclassical model of carrier recombination in degenerate semiconductors and detailed in refs. [9–12] have been employed to estimate the donor-induced carrier density (n_d) and the renormalized band-gap energy (E_g), which are shown in panel (b) as a function of d_H. Three different d_H regions can be identified:

(i) *Low H-doses* ($d_H \leq 8z$, with $z = 1 \times 10^{15}$ ions cm^{-2}): At such doses, the high-energy edge of the PL band rigidly blueshifts, the emission efficiency begins to decrease, and a new band appears at low energy (as shown by misfits in the simulated spectra). These effects are due to the formation of H-related donor states with an ensuing increase in n_d (up to a factor of 20) at almost constant value of E_g; see arrows in the figure and ref.[9].

(ii) *Intermediate H-doses* ($8z < d_H \leq 50z$): For d_H just larger than $8z$, the PL spectrum abruptly narrows and almost rigidly blueshifts. *The carrier density initially decreases* (by a factor of 4) *and then keeps constant, while the band-gap energy continuously increases.* The band gap opens by as much as $\Delta E_g = 0.4$ eV—independently of the ion-current and ion-energy values employed in the hydrogenation process—for an increase in d_H of about a factor of 6, whilst the PL integrated intensity decreases by roughly a factor of 20.

(iii) *High H-doses* ($50z < d_H \leq 1000z$): The H-induced effects resemble, to a much smaller extent, those in the low H-doses regime: n_d doubles while E_g just slightly increases and the PL integrated intensity keeps constant.

The robustness of the band-gap opening at intermediate H-doses is supported by the room-temperature[13] current–voltage characteristic and estimated sample conductivities (σ) shown in **Figure 2**. At low H-doses, σ increases and reaches a peak at $d_H = 8z$, which parallels the dependence of n_d on d_H shown in Figure 1b. At intermediate H-doses, σ first decreases (by a factor of 4), then slightly increases and saturates (or decreases) at high H-doses ($d_H > 50z$). These transport measurements confirm that at intermediate H-doses the PL spectrum *blueshifts* whilst the carrier density *decreases*. These features indicate a *real band-gap opening, different from a mere band-filling effect*. It is different, indeed, from the Moss–Burstein shift, reported in degenerate InN[14–16] and accounting for the moderate PL peak blueshift observed here at low and high H-dose regimes; see Figure 1.

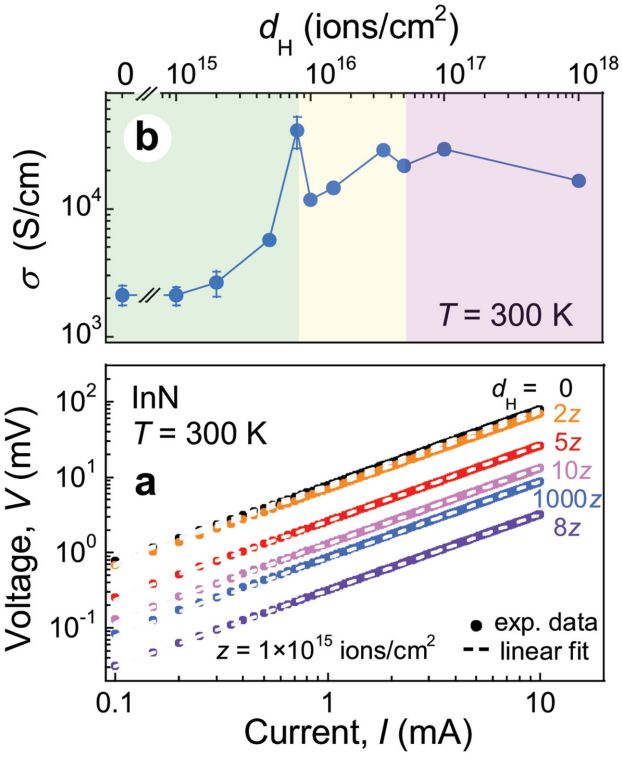

Figure 2. Conductivity measurements on hydrogenated InN. a) Room-temperature current–voltage characteristics (full dots) of an InN epilayer postgrowth treated with different H-dose (d_H). Dashed lines are linear fits of the data. b) Estimated layer conductivity (σ) as a function of d_H. Shaded colored areas identify the three d_H regions described in the text.

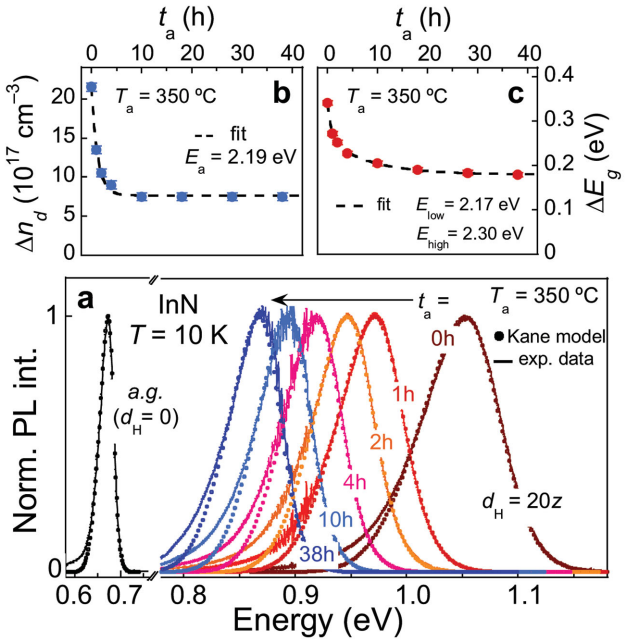

Figure 3. Thermal stability studies of the band-gap opening. a) Low-temperature (T = 10 K) normalized PL spectra (solid lines) and simulations (full dots) of a hydrogenated (d_H = 20z) InN epilayer subjected to thermal annealing at T_a = 350 °C for increasing times (t_a). The as-grown (a.g.) sample is also shown for comparison's purposes. Features at ≈0.9 eV are due to atmospheric absorption. b) H-induced increase in the carrier density (Δn_d) and c) in the renormalized band-gap energy (ΔE_g) as a function of t_a. Error bars are within the symbol size. Dashed lines are Arrhenius-like fits to the data; see text and ref.[9]. The best-fit values of deactivation energy for the H-induced effects are also given.

Additional information on the origin of the H-induced effects is provided by the analysis of the changes in the PL spectra upon isothermal annealing at T_a = 350 °C for increasing time intervals (t_a). As an example, the PL spectra of a same sample untreated, then hydrogenated at d_H = 20z—namely, at a d_H in the middle of the intermediate range at which the band gap widely opens—and finally annealed, are shown in **Figure 3**a together with their simulations by the Kane semiclassical model. Upon annealing, the PL spectrum tends to recover the line-shape of the untreated sample: It narrows (i.e., n_d decreases; see panel (b)); it redshifts (i.e., the band gap closes; see panel (c)); and the PL efficiency increases (not shown here). This recovery process saturates after a few hour annealing, without achieving a full restoration of the PL spectrum. There are, therefore, two different defects (at least) accounting for the observed H-induced effects: H-complexes dissociating already at T_a = 350 °C, and secondary, more stable H-related defects persisting after 40 h at T_a = 350 °C. Irradiations with He-atoms had also been performed to purposely and controllably damage the sample without chemical interactions, in order to support the interpretation of the two components of the band-gap opening in terms of formation of H-complexes and of structural damage, respectively; see Section S1 (Supporting Information). The origin of the latter effect will be discussed later.

The decrease in carrier density (Δn_d) upon increasing thermal annealing time t_a (see Figure 3b) is attributed to a thermal dissociation of the H-complexes, followed by H-atom out-diffusion.[9] It is modeled by an Arrhenius-like law, as explained in details in ref.[9], with an activation energy E_a = 2.19 ± 0.01 eV.[17] The residual value of Δn_d at saturation is ascribed to the formation of donor N-vacancies during the hydrogenation process.[9,18] Similarly, the decrease upon annealing of the InN band-gap opening is well fitted in terms of H-complexes dissociation; see dashed line in Figure 3c. Two activation energies (E_{low} = 2.17 ± 0.02 eV and E_{high} = 2.30 ± 0.02 eV) are estimated in this case.

H-effects similar to those reported so far are observed also in In-rich (InGa)N alloys. There, the PL peak energy (E_{peak}) *blueshifts monotonically with increasing* d_H at a rate decreasing with decreasing In-concentration (x) and vanishing for $x \approx 0.5$; see Section S2 (Supporting Information).

2.2. Solitary-Cation Model

The microscopic nature of the band-gap opening experimentally observed in InN has been investigated by a theoretical detailed survey of different defects that may form in this hydrogenated compound. First, we investigated a single H-atom located at different sites: The interstitial bond-center (BC) site, the antibonding (AB) site, and the N-substitutional site.[19] In agreement with previous studies, H-atoms located at these sites induce donor levels in the conduction band (CB), with ensuing band-filling effects.[19,20] They have no effect, instead, on the host band-gap energy.

Then, we considered an H_{BC}–$3H_{ab}$ donor complex (the upper- and lower-case letters refer, respectively, to H bonds parallel and perpendicular to the wurtzite c-axis), which consists of four H-atoms bound to four N-atoms nearest-neighbors of an In-atom, as shown in **Figure 4**a. This complex forms in hydrogenated In-rich (InGa)N alloys, where its structural properties were extensively investigated by DFT (density functional theory), EXAFS (extended X-ray absorption fine structure), and XANES (X-ray absorption near edge structure) studies.[21] The H_{BC}–$3H_{ab}$ complex has been considered here because the observation that hydrogen irradiation produces similar effects in InN and In-rich (InGa)N alloys (see Section S2, Supporting Information) supports its formation in InN, too. The peculiar atomic arrangement of the H_{BC}–$3H_{ab}$ complex gives rise to an effective *screening* of the surrounding crystal environment and generates a *solitary cation* at its center, as unveiled here by combining an analysis of the complex geometry with a detailed study of its electronic structure and chemical bonding. From a structural point of view, the formation of three N—H_{ab} bonds induces a strong elongation of the corresponding In*–N distances, where In* is the In-atom at the center of the H_{BC}–$3H_{ab}$ complex; see Figure 4a. In turns, this implies a significant weakening of the three In*—N bonds, as shown by a displacement of the electronic charge from these bonds to the N—H_{ab} bonds; see Figure 4b. Moreover, the fourth H-atom, H_{BC}, breaks the fourth In*—N bond and interacts quite markedly with the N-atom to form a strong N—H_{BC} bond. The *cooperative action* of the four H-atoms in the complex substantially separates the In*-cation from its environment. This cation is similar to an isolated atom in bulk InN, as shown in Figure 4b by the almost

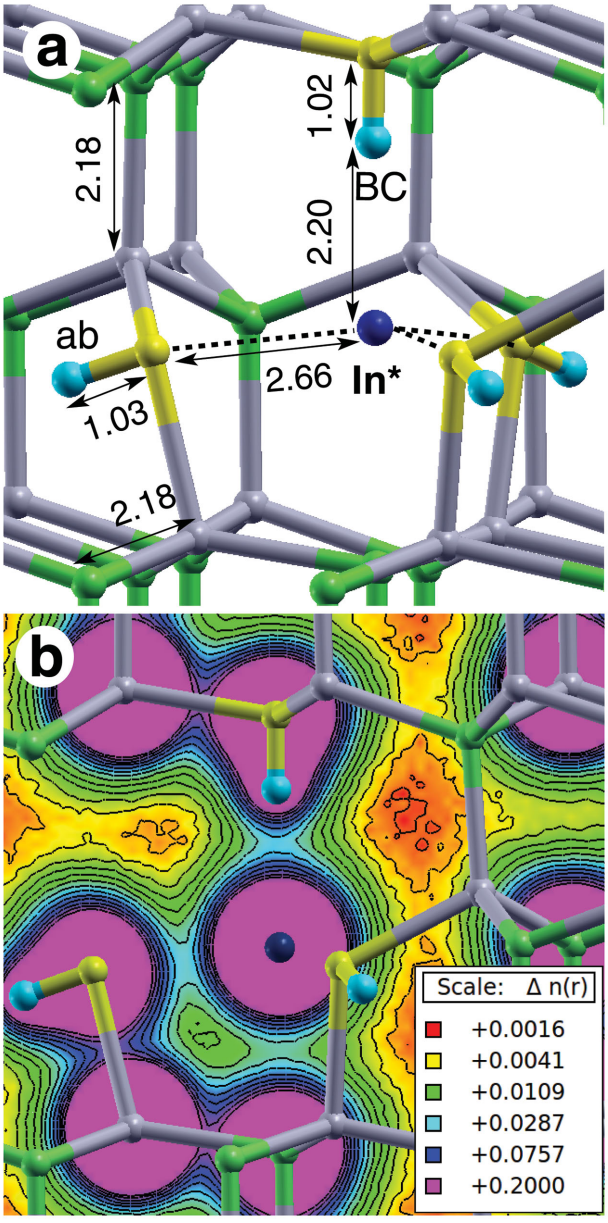

Figure 4. H_{BC}–$3H_{ab}$ complex and In* solitary cation. a) Geometry of the H_{BC}–$3H_{ab}$ complex (in an InN matrix). The four H-atoms and the four N-atoms involved in the complex are represented by light-blue and yellow spheres, respectively. The In-atom separated from its environment (In*) is represented by a dark-blue sphere. In and N atoms of the bulk InN are represented by grey and green spheres, respectively. BC and ab labels identify, respectively, bond-centered and antibonding sites of the H-atoms. The N—H_{BC} bond is along the wurtzite *c*-axis. Bond distances are given in angstroms. b) Isoelectronic contours of the total charge density taken on the plane identified by the pair of N—H_{BC} and N—H_{ab} bonds indicated in panel (a). Color-code for the isoelectronic contour is displayed in the inset; values are in e $Bohr^{-3}$ units. Note that some atoms are dropped from the figure in order to ease the view of the structure.

spherical symmetry of the charge density surrounding In*. The signature of the genesis of an In* solitary cation is given by the appearance of an atomic-like *s*-state, *s*(In*), which is: (i) strongly localized at the In*-site in the real space, as shown in **Figure 5**b by the plot of the square modulus of the corresponding electronic single-particle state, and (ii) energetically close to the valence band maximum (VBM), see the red bold line in Figure 5a showing that this state smoothly follows the top of the valence band in reciprocal space. Thus, the *s*(In*) energy level is well below that of the delocalized *s*-states of the unperturbed In-atoms, *s*(In), which mostly contribute to the conduction band minimum (CBM). The density of states projected on Löwdin atomic *s*-orbitals (pDOS) of In* and unperturbed In-atoms, respectively, support the above picture by showing that the *s*(In*)-states are located close to the VBM, while the *s*(In)-states form the CBM; see the upper panel of Figure 5c. Finally, the four electrons introduced by the four H-atoms of the H_{BC}–$3H_{ab}$ complex are divided in two pairs that occupy the *s*(In*)-state and the CBM. This corresponds to a formal change in the atomic charge of an In-atom from +3 (in the unperturbed In cations) to +1 (in the In* solitary cations), thus highlighting the sizable modification in the chemical properties of a material's constituent atom produced by the hydrogen insertion in the host lattice.

We will now demonstrate that the formation of the In* solitary cation by the coordinated action of four H-atoms and the ensuing presence of the *s*(In*)-state are the key conditions for the occurrence of a band-gap opening at the Γ point. Let us consider a hypothetical defect structure where the H_{BC}–$3H_{ab}$ geometry is maintained but the four H-atoms are removed from their sites (hereafter referred to as $\underline{\underline{H}}_{BC} - 3\underline{\underline{H}}_{ab}$ configuration). In this configuration, the interaction of the In*-atom with its N-neighbors is partially recovered and the In* loses its isolated-atom character. In this case, the *s*(In*)-state leaves the VBM to join the *s*(In)-states at the CBM (see lower panel of Figure 5c) and the pristine band-gap energy of InN is almost restored, but for residual strain effects; see also the band-edge alignments between the band structures of the pristine and defected InN host calculated at the Γ point and sketched in **Figure 6**. Finally, this same figure shows that the *CBM raises* when the *s*(In*)-state occurs in the system. Therefore, the observed band-gap opening can be accounted for by a level-band anticrossing model involving the *s*(In*)-state and the *s*(In)-states of the CB edge.

A band-gap increase $\Delta E_g = 0.26$ eV is theoretically estimated for an In*-concentration ([In*]) of about 10^{20} atoms cm^{-3}; see Section S3 (Supporting Information). This condition favorably compares with the experimental findings, in particular with a band-gap increase of ≈0.2 eV that can be attributed to the H-complex mentioned above; see Figures 1 and 3. Thus, a significant increase in the band-gap energy can be achieved provided that a large [In*] is reached—namely a high concentration of atomic H ([H]) in bulk InN. Such high values of [H] may be justified by the small values of band-gap energy and bulk modulus in InN (≈0.6 eV and 140 GPa, respectively)—which imply a relatively low-energy cost for the formation of H^+ species—as well as by the local strain accompanying the formation of H^+–N bonds; see Section S4 (Supporting Information). The occurrence of such favorable conditions for the introduction of hydrogen in InN is well exemplified by a comparison with a material, GaN, characterized by larger values of band-gap energy and bulk modulus (≈3.4 eV and 210 GPa, respectively). At $T = 300$ K, we estimate indeed a [H^+] value in GaN several (≈12) orders of magnitude

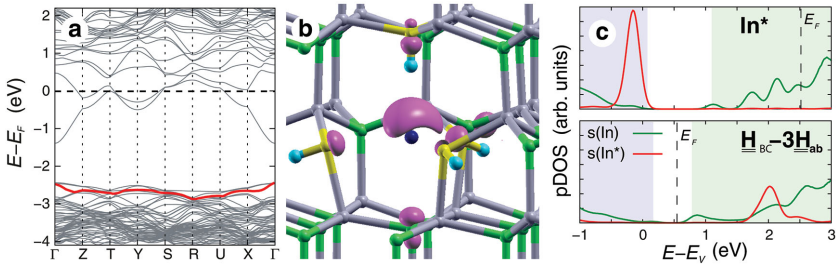

Figure 5. Electronic features of the In* solitary cation. a) Dispersion curves of the electronic states in the Brillouin zone for the In* in bulk InN. The Fermi energy (E_F) is within the conduction band. The red bold curve identifies the electronic *s*(In*)-state induced by the In* solitary cation. b) Charge density relative to the *s*(In*) single-particle state highlighted in panel (a). The value of the isosurface corresponds to $7 \times 10^{-3}e$ Bohr^{-3}. c) Portions of the density of states as projected on *s* atomic orbitals of the In* and unperturbed In-atoms (pDOS) for the In* structure (upper panel) and for the defect structure with H-atoms stripped off ($\underline{H}_{BC} - 3\underline{H}_{ab}$ complex, lower panel). The shaded blue and green areas identify the energy regions pertaining to valence and conduction bands, respectively. Energies are given with respect to the valence band edge of the pristine InN (E_V), as in Figure 6.

smaller than that in InN. These results also account for the experimental observations of a progressive reduction of the band-gap opening effect in (InGa)N alloys with increasing Ga-concentration, with a vanishing for ≈50% of [Ga]; see Section S2 (Supporting Information). In fact, though solitary cations (Ga*) are predicted to form even in GaN—with an effect on the GaN band-gap energy similar to that In* has on the InN one—higher formation energies for isolated H lead to low values of [H] and, consequently, of [Ga*]. This prevents the achievement of a band-gap opening in GaN as well as in Ga-rich (InGa)N alloys; see Section S4 (Supporting Information).

An In* solitary cation would also qualitatively account for the observation of the peculiar, abrupt raise with a following saturation in the InN band-gap energy and the concurrent decrease in the carrier density above a critical H-dose; see Figure 1. In the former case, the concentration of In* cations (namely, the concentration of H_{BC}–$3H_{ab}$ complexes) should be proportional to $[H]^4$, whilst the saturation of the band-gap opening shown in Figure 1b is accounted for by a quick increase in the In* formation energy with increasing [In*] because of the local strain accompanying the In*-structure formation; see Section S5 (Supporting Information). As regards the decrease in the carrier density that parallels the band-gap opening (see Figures 1b and 2b), it is explained by the electronic features of In*: Only two free-electrons are produced when an H_{BC}–$3H_{ab}$ complex forms—other two electrons occupy the *s*(In*)-state close to the VBM—while four isolated H_{BC} or H_{ab} atoms in InN give rise to four free-electrons in the CB.

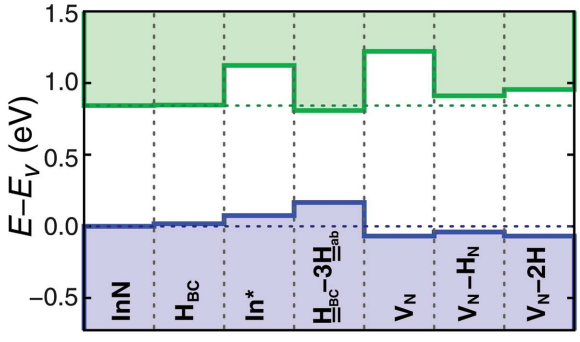

Figure 6. Band line-ups of pristine and defected InN. Blue and green lines identify the valence and conduction band edges at the Γ point, respectively, for each defect structure investigated; see the text. The horizontal dashed lines identify the valence and conduction band edges of pristine InN. V_N–2H and V_N–H_N represent complexes formed by a V_N and two H-saturators of In dangling bonds and by a V_N with a H-atom (H_N) at the site of the vacant N, respectively. Band alignments are calculated in the 96-atom supercells, that is, for a defect concentration of 6×10^{20} cm^{-3}. Energies are given with respect to the valence band edge of the pristine InN (E_V), as in Figure 5c.

2.3. H-Related Defects

On reporting previously on the donor nature of interstitial H atoms in *n*-type InN,[9] we observed a side effect of hydrogenation treatment, namely, a small structural sample damage with likely formation of nitrogen vacancies.[9,18] This effect was disclosed by comparing the behavior under annealing of two samples, one bombarded with chemically inactive He-ions, the other irradiated with H-ions;[9,21] see also Section S1 (Supporting Information). Pure damage effects are stable upon mild thermal ($T_a \approx 350$ °C) annealing at which H-complexes normally dissociate in semiconductors (e.g., H–N complexes in III-N-V dilute nitrides)[22–25] and H-effects are fully reversed. In the present case of a band-gap opening in InN upon hydrogenation, a large but not complete recovery of the original band gap upon mild thermal annealing (see Figure 3) indicates once more that H-bonds are involved in the observed phenomenon and that side damaging effects are induced by hydrogenation. Such effects have led us to search for defects, other than the H_{BC}–$3H_{ab}$ or other H-complexes, that may form upon hydrogenation, open the band gap, and be stable upon annealing.

In this regard, we focus on nitrogen-vacancies (V_N) and In-interstitials (In_{int}). Those hard defects are characterized by the smallest formation energies among different, native defects in InN[19] and have been proposed to form upon hydrogenation.[9,18] As regards In_{int}, present results confirm its stable split configuration with a donor level within the CB, in agreement with previous studies,[19,20] *while they show no effect on the band-gap energy*. On the other hand, V_N's induce a relevant increase in the band-gap energy—up to about 0.4 eV for a V_N concentration $[V_N]$ of 6×10^{20} cm^{-3}; see Figure 6—but the extent of such an increase critically depends on $[V_N]$; see Section S5 (Supporting Information). Therefore, the residual band-gap opening observed after the long thermal annealing is tentatively ascribed to the presence of V_N's provided their concentration upon hydrogen irradiation be high enough.[18] Moreover, it should be noted that only naked V_N's contribute to the band-gap opening because hydrogen neutralizes such an effect by forming V_N–2H or V_N–H_N complexes; see Figure 6 and Section S6 (Supporting Information).

3. Conclusion

In conclusion, the *genesis of solitary cations* and the consequent changes in the band-gap energy observed and/or predicted in several topical nitrides—i.e., InN, GaN, and (InGa)N alloys—demonstrate that the fundamental properties of these semiconductors can be modified by a direct change of the chemistry of their constituent cations by means of atomic hydrogen. In particular, the peculiar atomic arrangement of four H-atoms around an In-atom in the H_{BC}–$3H_{ab}$ complex screens the In atom from the surrounding crystal environment through the formation of four strong N—H bonds and generates, therefore, a solitary In* cation. Such an arrangement deeply affects the fundamental electronic properties of the host crystal: The band anticrossing interaction of the In* atomic-like electronic states with those of the conduction band minimum of the materials leads to a genuine and large band-gap opening, an effect with the distinctive feature to be reversible. Finally, a high concentration of In solitary cations might explain values of the InN band-gap energy greater than 1 eV, sometime reported in films with low carrier concentrations ($<10^{19}$ cm^{-3}) grown by sputtering techniques and long debated in the literature.[26–30]

The reported band-gap opening in In-rich (InGa)N alloys, together with the possibility of a fine tuning by varying H-dose and/or In-content, indicate a novel route for a *tuneable, post-growth band-gap engineering* in nitride semiconductors.

4. Experimental Section

Sample Growth and Hydrogen Incorporation: The samples studied here are a 500 nm thick InN (IW358) and a series of 25 nm thick $In_xGa_{1-x}N$ ($0.43 \leq x \leq 0.85$) epilayers grown by plasma-induced molecular beam epitaxy on a sapphire substrate with GaN and AlN buffer layers. Details on the sample characteristics and growth are reported in refs. [12,31,32]. All samples have been irradiated with different H-doses (1×10^{14} ions $cm^{-2} \leq d_H \leq 1 \times 10^{18}$ ions cm^{-2}) by means of a Kaufman ion source.[33] The ion-beam kinetic energy was set to low values (10–100 eV) in order to minimize sample damage whilst the samples were kept at a temperature of 300 °C during the whole irradiation process to increase H-diffusion.

Optical and Transport Characterization: The effects of solitary cations formation have been probed by PL and conductivity measurements. Photoluminescence has been excited by an Ar^+ (λ_{exc} = 514 nm) or an Nd:YVO_4 (λ_{exc} = 532 nm) laser, dispersed by a 0.25 m focal-length or a 0.75 m focal-length monochromator, and detected by a liquid-nitrogen-cooled InGaAs photodiode, an InGaAs array, or an Si charge-coupled-device, depending on the sample emission energy. All the spectra have been normalized to the optical setup response. Conductivity measurements have been taken in a four-point collinear geometry[34,35] by using a high-impedance system.

Theoretical Calculations: Simulations of both wurtzite InN and GaN have been performed by using the Quantum-ESPRESSO suite of programs,[36] ultrasoft pseudopotentials,[37,38] with plane-waves cut-offs of 30 Ry for wave functions and of 180 Ry for densities. The electronic channels considered in the atomic pseudopotentials were 2*s* and 2*p* for N, 3*d*, 4*s*, and 4*p* for Ga, and 4*d*, 5*s*, and 5*p* for In. In order to correct the vanishing band gap of typical density functional theory (DFT) simulations of InN, the Hubbard-U correction[39,40] has been applied to the 3*d* and 4*d* states of Ga and In, respectively, and to the 2*p* states of N. Similarly to what already done in GaN and (InGa)N alloys,[27,41] the U value was found parametrically for In, Ga, and N, by reproducing the experimental values of the band-gap energy and of the position of the Ga and In *d*-shell in the density of states with respect to the top of the valence band (a four-atom hexagonal unit cell with a $6 \times 6 \times 6$ k-point mesh was used). The obtained *U* values are $U_{N(2p)}$ = 4.0 eV, $U_{Ga(3d)}$ = 8.0 eV, and $U_{In(3d)}$ = 1.0 eV. With these choices, lattice parameters, band-gap energies, and bulk moduli deviate from experimental values by at most 0.7%, 10%, and 5%, in the order. The results reported in the text, unless otherwise stated, refer to 96-atom supercells, built from $2 \times 3 \times 2$ times the eight-atom orthorhombic unit cell. Geometry optimizations were performed for all the structures by minimizing the atomic forces, fully relaxing the positions of all the supercell atoms, and using a $2 \times 2 \times 2$ k-point Monkhorst–Pack mesh, Γ point included. Dispersion curves have been calculated by nonself-consistent diagonalization of a potential obtained by means of a $3 \times 3 \times 3$ k-point Monkhorst–Pack mesh, Γ point included. Effects of concentration have been checked by using different size supercells: A 72-atom hexagonal supercell ($3 \times 3 \times 2$ times the four-atom hexagonal unit cell), a 128-atom, and a 360-atom (respectively $2 \times 4 \times 2$ and $3 \times 3 \times 5$ times the eight-atom orthorhombic supercell). The electronic results obtained from Hubbard-U calculations have been checked, for 72-atom supercells, against hybrid density functional calculations with the Heyd–Scuseria–Ernzerhof (HSE) exchange-correlation formulation.[42,43] HSE calculations were performed with norm-conserving Hartwigsen–Goedecker–Hutter pseudopotentials,[44] 80 Ry cutoff, $2 \times 2 \times 2$ k-point Monckhorst–Pack mesh. A substantial and satisfactory agreement between the two formulations has been found and therefore the much lighter and faster Hubbard-U approach has been used throughout.

Supporting Information

Supporting Information is available from the Wiley Online Library or from the author.

Acknowledgements

This work was partially supported by EU (under Grant Agreement No. PIEF-GA-2010-272612), by Italian MIUR (under FIRB project DeLIGHTeD, Prot. RBFR12RS1W), and by EPSRC (EP/J015296/1). The authors are grateful to M. De Luca (Sapienza University of Rome) and O. Makarovsky (The University of Nottingham) for useful discussions, and to J.C. Maan (HFML of Nijmegen), A. Selloni (Princeton University), and G. Ciatto (Synchrotron SOLEIL) for a critical reading of the manuscript and valuable comments.
Note: This article was originally published in greyscale. Acknowledgements were amended and the article was published in color on September 2, 2015.

Received: May 5, 2015
Revised: June 26, 2015
Published online: July 27, 2015

[1] J. I. Pankove, N. M. Johnson, *Hydrogen in Semiconductors*, Semiconductors and Semimetals, Vol. 34, Academic Press, New York, NY, USA **1991**.
[2] S. J. Pearton, J. W. Corbett, M. Stavola, *Hydrogen in Crystalline Semiconductors*, Springer Series in Materials Science, Vol. 16, Springer-Verlag, Berlin, Germany **1992**.
[3] C. G. Van de Walle, B. Tuttle, *IEEE Trans. Electron Devices* **2000**, *47*, 1779.
[4] S. Nakamura, N. Iwasa, M. Senoh, T. Mukai, *Jpn. J. Appl. Phys.* **1992**, *31*, 1258.
[5] E. Burstein, *Phys. Rev.* **1954**, *93*, 632.
[6] T. S. Moss, *Proc. Phys. Soc. London, Sect. B* **1954**, *67*, 775.

[7] R. Trotta, A. Polimeni, F. Martelli, G. Pettinari, M. Capizzi, L. Felisari, S. Rubini, M. Francardi, A. Gerardino, P. C. M. Christianen, J. C. Maan, *Adv. Mater.* **2011**, *23*, 2706, and references therein.
[8] N. Balakrishnan, G. Pettinari, O. Makarovsky, L. Turyanska, M. W. Fay, M. De Luca, A. Polimeni, M. Capizzi, F. Martelli, S. Rubini, A. Patanè, *Phys. Rev. B* **2012**, *86*, 155307.
[9] G. Pettinari, F. Masia, M. Capizzi, A. Polimeni, M. Losurdo, G. Bruno, T. H. Kim, S. Choi, A. Brown, V. Lebedev, V. Cimalla, O. Ambacher, *Phys. Rev. B* **2008**, *77*, 125207.
[10] We use the same parameters and routine for spectra simulation used in ref. [9], but for the values of hole and electron effective masses, for which we use, respectively, a more updated value ($m_h = 0.42\ m_0$; see ref. [11]) and the lower limit we directly derived in the same InN (IW358) sample by magneto-optical studies ($m_e = 0.093\ m_0$; see ref. [12]).
[11] X. Wang, S.-B. Che, Y. Ishitani, A. Yoshikawa, *Appl. Phys. Lett.* **2008**, *92*, 132108.
[12] G. Pettinari, A. Polimeni, M. Capizzi, J. H. Blokland, P. C. M. Christianen, J. C. Maan, V. Lebedev, V. Cimalla, O. Ambacher, *Phys. Rev. B* **2009**, *79*, 165207.
[13] Due to the decrease of PL efficiency in hydrogenated samples (see Figure 1) and to experimental limitations, conductivity measurements and PL spectra analysis have been performed at different temperature (300 K and 10 K, respectively). Nevertheless, the relative variations of the obtained sample conductivity and H-induced carrier density for increasing d_H are in good agreement. This also supports the use of a same electron effective mass value in the simulation of the PL spectra treated with different d_H.
[14] S. P. Fu, T. T. Chen, Y. F. Chen, *Semicond. Sci. Technol.* **2006**, *26*, 244.
[15] J. S. Thakur, Y. V. Danylyuk, D. Haddad, V. M. Naik, R. Naik, G. W. Auner, *Phys. Rev. B* **2007**, *76*, 35309.
[16] M. Tangi, J. Kuyyalil, S. M. Shivaprasad, *J. Appl. Phys.* **2013**, *114*, 153501.
[17] Notice that, differently from ref. [9], it is possible to identify here only one activation energy (most likely associated with the nitrogen-antibonding complex dissociation; see ref. [9]). Indeed, under the employed thermal annealing conditions (T_a = 350 °C), the effect of the bond-center (BC) H-complex—identified in ref. [9] as coresponsible of the carrier density increase upon hydrogenation—is not detectable because of its small activation energy (≈1.97 eV; see ref. [9]), which would reduce the density of the BC H-complexes to ≈1% its initial value just after 5 min of annealing.
[18] M. Losurdo, M. M. Giangregorio, G. Bruno, T.-H. Kim, S. Choi, A. S. Brown, G. Pettinari, M. Capizzi, A. Polimeni, *Appl. Phys. Lett.* **2007**, *91*, 081917.
[19] C. G. Van de Walle, J. L. Lyons, A. Janotti, *Phys. Status Solidi A* **2010**, *207*, 1024.
[20] A. Janotti, J. L. Lyons, C. G. Van de Walle, *Phys. Status Solidi A* **2012**, *209*, 65.
[21] M. De Luca, G. Pettinari, G. Ciatto, L. Amidani, F. Filippone, A. Polimeni, E. Fonda, F. Boscherini, A. A. Bonapasta, D. Giubertoni, A. Knubel, V. Lebedev, M. Capizzi, *Phys. Rev. B* **2012**, *86*, 201202R.
[22] M. Bissiri, G. Baldassarri Höger von Högersthal, A. Polimeni, V. Gaspari, F. Ranalli, M. Capizzi, A. A. Bonapasta, F. Jiang, M. Stavola, D. Gollub, M. Fischer, M. Reinhardt, A. Forchel, *Phys. Rev. B* **2002**, *65*, 235210.
[23] A. Polimeni, M. Bissiri, M. Felici, M. Capizzi, I. A. Buyanova, W. M. Chen, H. P. Xin, C. W. Tu, *Phys. Rev. B* **2003**, *67*, 201303.
[24] G. Baldassarri Höger von Högersthal, M. Bissiri, A. Polimeni, M. Capizzi, M. Fischer, M. Reinhardt, A. Forchel, *Appl. Phys. Lett.* **2001**, *78*, 3472.
[25] G. Ciatto, *Hydrogenated Dilute Nitride Semiconductors – Theory, Properties and Applications*, Pan Stanford Publishing, Singapore **2015**.
[26] K. S. A. Butcher, H. Hirshy, R. M. Perks, M. Wintrebert-Fouquet, P.T.-T Chen, *Phys. Status Solidi A* **2006**, *203*, 66, and references therein.
[27] P.T.-T. Chen, J. E. Downes, A. J. Fernandes, K. S. A. Butcher, M. Wintrebert-Fouquet, R. Wuhrer, M. R. Phillips, *Thin Solid Films* **2011**, *519*, 1831.
[28] K. S. A. Butcher, T. L. Tansley, *Superlattices Microstruct.* **2005**, *38*, 1, and references therein.
[29] W. Walukiewicz, J. W. AgerIII, K. M. Yu, Z. Liliental-Weber, J. Wu, S. X. Li, R. E. Jones, J. D. Denlinger, *J. Phys. D: Appl. Phys.* **2006**, *39*, R83, and references therein.
[30] P. D. C. King, T. D. Veal, P. H. Jefferson, S. A. Hatfield, L. F. J. Piper, C. F. McConville, F. Fuchs, J. Furthmüller, F. Bechstedt, H. Lu, W. J. Schaff, *Phys. Rev. B* **2008**, *77*, 045316.
[31] V. Lebedev, V. Cimalla, T. Baumann, O. Ambacher, F. M. Morales, J. G. Lozano, D. González, *J. Appl. Phys.* **2006**, *100*, 094903.
[32] V. Lebedev, V. M. Polyakov, S. Hauguth-Frank, V. Cimalla, Ch. Y. Wang, G. Ecke, F. Schwierz, A. Schober, J. G. Lozano, F. M. Morales, D. González, O. Ambacher, *J. Appl. Phys.* **2008**, *103*, 073715.
[33] A. Kaufman, *Rev. Sci. Instrum.* **1990**, *61*, 230.
[34] L. B. Valdes, *Proc. IRE* **1954**, *42*, 420.
[35] F. M. Smits, *Bell Syst. Tech. J.* **1958**, *37*, 711.
[36] P. Giannozzi, S. Baroni, N. Bonini, M. Calandra, R. Car, C. Cavazzoni, D. Ceresoli, G. L. Chiarotti, M. Cococcioni, I. Dabo, A. Dal Corso, S. de Gironcoli, S. Fabris, G. Fratesi, R. Gebauer, U. Gerstmann, C. Gougoussis, A. Kokalj, M. Lazzeri, L. Martin-Samos, N. Marzari, F. Mauri, R. Mazzarello, S. Paolini, A. Pasquarello, L. Paulatto, C. Sbraccia, S. Scandolo, G. Sclauzero, A. P. Seitsonen, A. Smogunov, P. Umari, R. M. Wentzcovitch, *J. Phys.: Condens. Matter* **2009**, *21*, 395502.
[37] D. Vanderbilt, *Phys. Rev. B* **2009**, *41*, 7892.
[38] a) A. M. Rappe, K. M. Rabe, E. Kaxiras, J. D. Joannopoulos, *Phys. Rev. B* **1990**, *41*, 1227; b) A. M. Rappe, K. M. Rabe, E. Kaxiras, J. D. Joannopoulos, *Phys. Rev. B* **1991**, *44*, 13175(E).
[39] V. I. Anisimov, F. Aryasetiawan, A. I. Lichtenstein, *J. Phys.: Condens. Matter.* **1997**, *9*, 767.
[40] M. Cococcioni, S. de Gironcoli, *Phys. Rev. B* **2005**, *71*, 035105.
[41] F. Filippone, G. Mattioli, P. Alippi, A. Amore Bonapasta, *Phys. Rev. Lett.* **2011**, *107*, 196401.
[42] J. Heyd, G. E. Scuseria, M. Ernzerhof, *J. Chem. Phys.* **2003**, *118*, 8207.
[43] X. Wu, E. J. Walter, A. M. Rappe, R. Car, A. Selloni, *Phys. Rev. B* **2009**, *80*, 115201.
[44] C. Hartwigsen, S. Goedecker, J. Hutter, *Phys. Rev. B* **1998**, *58*, 3641.